Near wake analysis of actuator line method immersed in turbulent flow using large-eddy simulations

Jörn Nathan[1], Christian Masson[1], and Louis Dufresne[1]

[1]ÉTS, Univ. du Québec, Mechanical Engineering, Montréal H3C 1K3, Canada

Correspondence to: Jörn Nathan (joern.nathan.1@ens.etsmtl.ca)

Abstract. The interaction between wind turbines through their wakes is an important aspect of the conception and operation of a wind farm. Wakes are characterized by an elevated turbulence level and a ~~noticable~~ noticeable velocity deficit which causes a decrease in energy output and fatigue on downstream turbines. In order to gain a better understanding of this phenomenon this ~~works~~ work uses large-eddy simulations together with an actuator line model and different ambient ~~turbulences~~ turbulence imposed as boundary conditions. This is achieved by using the SOWFA framework from NREL (USA) which is first validated against another popular CFD framework for wind energy, EllipSys3D, and then verified against the experimental results from the MEXICO and NEW MEXICO wind tunnel experiments. By using the predicted torque as a global indicator, the optimal width of the distribution kernel for the actuator line is determined for different grid resolutions. Then the rotor is immersed in homogeneous isotropic turbulence and a shear layer turbulence with different turbulence intensities, allowing to determine how far downstream the effect of the distinct blades is discernible. This can be used as an indicator for the extents of the near wake for different flow conditions.

1 Introduction

An important aspect for the conception of wind farms is the turbine spacing which depends on the interaction of wind turbines through their wakes. This phenomenon can decrease the wind park energy output by up to 20% due to the velocity deficit propagated by the wakes (Manwell et al., 2010). Additionally, it can increase the turbine fatigue due to the increased turbulence intensity. In order to study wake interactions, the flow around the rotor has to be modelled correctly. Hence the model should account for the apparition of turbulent structures of different magnitudes. For instance the vortices created by the blade tips and its interaction with the ambient turbulence.

As opposed to the far wake region (Olivares Espinosa, 2017), the near wake representation in a computational fluid dynamics simulation depends heavily on the applied rotor model. Approaches range from an actuator force representation inserted as momentum sink in the Navier-Stokes equations to full rotor modelling where the attached boundary layers on the blades are simulated (Sanderse et al., 2011). This work will apply the actuator line method (ALM) in order to model the transient behaviour of the rotor by representing distinctly the rotating blades as presented by Troldborg (2009). Each blade is represented by a force line allowing to reproduce the helicoidal vortical structure in the near wake allowing to ~~to~~ assess its interaction with the flow.

In order to evaluate the soundness of the present method a comparative study of the SOWFA framework, from NREL, and EllipSys3D, from DTU, was conducted as ~~initally~~ initially presented in Nathan et al. (2017). Based on this study, the method used throughout this work will be evaluated before proceeding to establish the base case for the non-turbulent inflow. For establishing the base case, the optimal width of the distribution kernel of the forces of the actuator line is determined. While previous work often focused on numerical stability as in Troldborg (2009) or Ivanell et al. (2010), when choosing the distribution width, Martínez-Tossas et al. (2015a) states that with decreasing distribution width, the line forces are getting too concentrated resulting in a wrong prediction of the rotor torque. Hence this work tries to evaluate the optimal width for each mesh resolution by using the predicted torque as a global indicator.

For the introduction of a turbulent inflow different methods exist for imposing a ~~stastically~~ statistically generated velocity field, such as inserting it via a momentum sink as done in Troldborg et al. (2011) or as boundary conditions as done in Olivares Espinosa (2017). This work adheres to the latter approach, as it was seen as more straightforward than the conversion of the velocity field to a force which then is translated back to the velocity field by the numerical solver~~as done the former approach~~.

Then shear layer turbulence (Muller et al., 2014) is introduced exposing the rotor model to a more realistic wind flow situation bearing more resemblance to applied wind energy. This novel approach takes into consideration the temporal evolution of the sheared velocity field, hence allowing it to be imposed as boundary condition as well. Also this method was not yet applied to the actuator line method.

Finally, the numerical results are used to examine the spatial extents of the near-wake region. While in previous work such as Krogstad and Eriksen (2013) or Sarmast et al. (2016) often the profiles of velocity deficits or turbulent kinetic energy are taken into consideration for evaluating the near-wake, this work uses the energy spectra to determine how far downstream the discernible effects of the distinct blades are ~~noticable~~noticeable. While the analysis of the turbulent inflow in previous work (Olivares Espinosa, 2017) has often been conducted using energy spectra, seldom energy spectra including the rotor effects are included in the analysis of the near-wake. As with increasing turbulence intensity the statistical convergence tends to be longer, the energy spectra approach in this work permits the analysis of the spatial extensions of the near-wake region even without fully convergence of second-order statistics.

2 Numerical methodology

The numerical simulations are based on the incompressible Navier-Stokes equations

$$\frac{\partial \mathbf{U}}{\partial t} + \nabla \cdot (\mathbf{U}\mathbf{U}) - \nabla \cdot (\nu \nabla \mathbf{U}) = -\nabla p/\rho + \mathbf{F} \quad (1)$$

$$\nabla \cdot \mathbf{U} = 0 \quad (2)$$

with $\mathbf{F}$ representing the actuator force inserted as a momentum sink, $\mathbf{U}$ ~~as~~ the velocity, $\nabla p/\rho$ ~~as~~ the modified pressure and ν ~~as~~ the kinematic viscosity. In section 2.1 the rotor model and the derivation of the force term $\mathbf{F}$ are discussed. Then in section 2.2

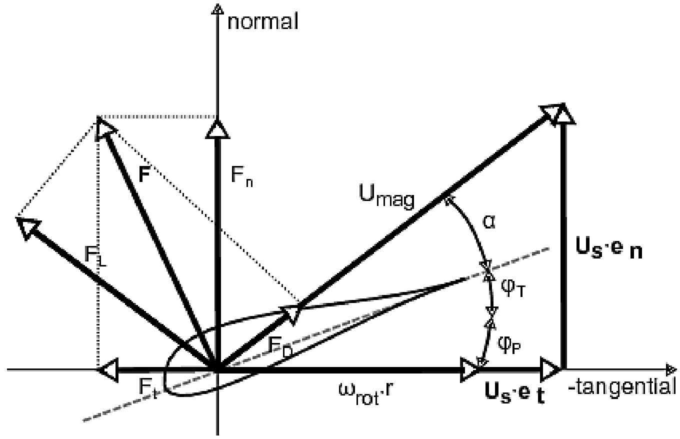

Figure 1. Geometry and forces in an airfoil section of the blade.

an overview is given on the methods generating the two different ambient turbulences turbulence and how they are imposed as boundary conditions. Finallythere is , a summary of the numerical framework and its setup is given in section 2.3.

2.1 Rotor model

The force term **F** in Eqn. (1) is obtained using

$$\mathbf{F} = \mathcal{G} * \left(f_{tip} \cdot (F_L \mathbf{e}_L + F_D \mathbf{e}_D)\right) \quad (3)$$

with the lift and drag forces shown in Figure (1) and defined as

$$F_L = \frac{1}{2}\, c_l\, U_{mag}^2\, c\, l_s \quad (4)$$

$$F_D = \frac{1}{2}\, c_d\, U_{mag}^2\, c\, l_s \quad (5)$$

with c_l and c_d as the lift and drag coefficient, U_{mag} the sampled velocity magnitude in the blade reference frame, c the chord width, l_s the length of the actuator segment, Gaussian kernel $\mathcal{G}$ the Gaussian kernel and tip correction (f_{tip} f_{tip}.

The same unmodified airfoil coefficients where selected among the ones presented in Schepers et al. (2012) based on the blade Reynolds number $Re = U_{mag}\, c/\nu$ with c as chord and ν as the kinematic viscosity. This used as shown in Shen et al. (2012) . These data was obtained from wind tunnel experiments 2D experiments without rotation in a wind tunnel and therefore it does not include the stall delay due to boundary layer stabilizing effects such as Coriolis and centrifugal forcing which enhance the lift of the airfoil (Vermeer et al., 2003) . In the case of the MEXICO rotor an adaption was proposed by Shen et al. (2012) circumventing this issue, but at the same time proposing a solution tuned for a known outcome. Hence this works adopts the unmodified 2D airfoil data .near the root of the blade. As shown in Nathan et al. (2017) using unmodified airfoil data results in problems predicting the blade forces in the root region for high wind speed flows, they seem to handle fairly well the moderate wind speeds which are in the focus of this work. Hence despite its shortcomings, the unmodified airfoil data is used throughout

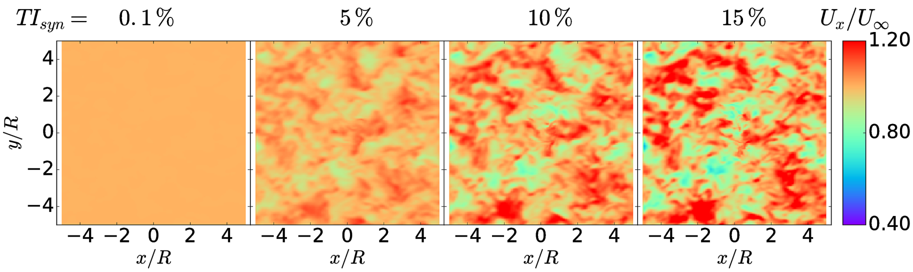

Figure 2. ~~Midplane~~ Mid-plane at ~~$y/R = 0$~~ $z/R = 0$ of instantaneous normalized axial velocity component U_x/U_∞ showing homogeneous isotropic turbulence for different turbulent intensities TI_{syn} in numerical domain.

this work. Then the forces in Eqn. (4) and Eqn. (5) are projected in the blade reference frame using the unit vectors $\mathbf{e}_L$ and $\mathbf{e}_D$ in Eqn. (3).

While the Glauert tip correction f_{tip} was originally intended (Glauert, 1935) to represent the otherwise absent tip vortices in the actuator disk model, it still proves advantageous for the ALM at lower resolutions as shown in Nathan (2018). Due to the relatively low resolution, the shed tip vortices from an ALM are much larger than the ones observed experimentally. Hence the induction caused by the simulated vortices is weaker than in reality and the Glauert tip correction permits to compensate for it (Nathan et al., 2017).

Finally in order to avoid spurious oscillations around the point of the inserted force, the punctual force is distributed using a kernel function $\mathcal{G} * (\cdot)$. As done in previous works such as Troldborg (2009) or Olivares Espinosa (2017) this work adheres to a normal distribution with the distribution width $\epsilon = \sigma \Delta x$ with σ the distribution width of the normal function and Δx the cell width.

2.2 Turbulence inflow generation

2.2.1 Homogeneous isotropic turbulence

A synthetic velocity field representing homogeneous isotropic turbulence based on the von-Kármán energy spectrum (Pope, 2000)

$$E(k) = \alpha \epsilon^{2/3} L^{5/3} \frac{L^4 \kappa^4}{(1 + L^2 \kappa^2)^{17/6}} \quad (6)$$

is obtained by using the algorithm proposed by Mann (1998). The technical details can be found in the article of Mann (1998) or more recently in Olivares Espinosa (2017). The main parameters for this approach are the integral length-scale L and the coefficient $\alpha \epsilon^{2/3}$ which can be used as a scaling factor to obtain the desired amplitude of the turbulent structures. The range of ~~wavenumber~~ wave number κ depends on the grid resolution and dimension extents. Hence, these parameters determine the ability of the numerical mesh to resolve a certain range of turbulent scales.

While several implementations of this method exist ~~e.g.~~ *e.g.* Olivares Espinosa (2017) or Muller et al. (2014), the implementation of Gilling (2009) was chosen for synthesizing the ~~HIT~~ homogeneous isotropic turbulence (HIT) for several reasons. It is

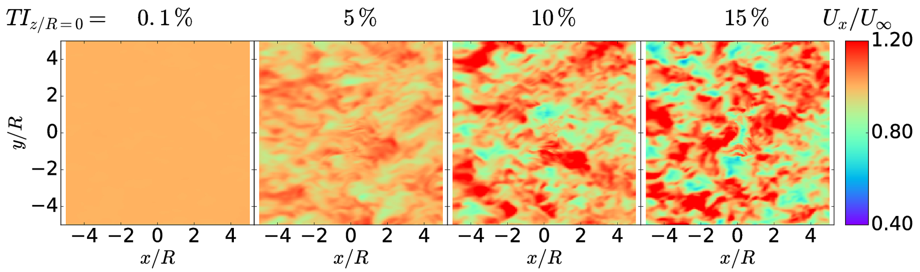

Figure 3. Horizontal plane of instantaneous axial velocity component U_x in sheared flow for different longitudinal turbulence intensities $TI_{z/R=0}$ at hub position.

in public domain, it corrects for a divergence free velocity field and allows to impose HIT at the boundaries at relatively low computational cost.

In Figure (2) the midplane of a generated turbulent field is shown for different turbulence intensities. The flow structures are identical apart from the different scaling of the velocity fluctuations. This results from using the same seed for the random number generator in the Mann algorithm and by scaling the obtained velocity field with $\alpha\epsilon^{2/3}$ to obtain the desired synthetic turbulence intensity TI_{syn}.

Contrary to Troldborg (2009) where the synthetic turbulence is imposed as a momentum source, in this work it is imposed as a boundary condition as done in Muller et al. (2014) and Olivares Espinosa (2017). The velocities are imposed by convecting the velocity field of the synthetic turbulence through the computational domain by the mean velocity U_∞ at each simulation time step. They are then projected by trilinear interpolation onto the computational points. In order to speed up the statistical convergence, the simulation is also initialized with the synthetic turbulence field.

2.2.2 Shear layer turbulence

Based on the Mann algorithm (Mann, 1998), Muller et al. (2014) developed a method to impose the synthetic turbulence on a sheared flow as boundary condition, including the evolution of the vortical structures. Apart from the turbulence intensity no further turbulence characteristics were published by Schepers et al. (2012). Hence a turbulence length scale of $R/4$ was chosen. These scales were larger than the width of the coarsest cells in the numerical mesh in order to dampen the effect of numerical dissipation in axial direction. A typical flow field generated by this algorithm can be seen in Figure (3) and Figure (4).

The mean velocity profile is obtained via the power law

$$U_x = U_{ref}\left(\frac{z}{z_{ref}}\right)^{\alpha_p} \quad (7)$$

hence the velocity at the bottom of the domain has not necessarily to be zero. Therefore the computational mesh can be much smaller than in a wall-resolved flow, as its mesh has to include the ground and has to have a high refinement in this region. The reference height z_{ref} was set at hub height and the reference velocity was set at $U_{ref} = 15\,m/s$. The parameter α_p can usually

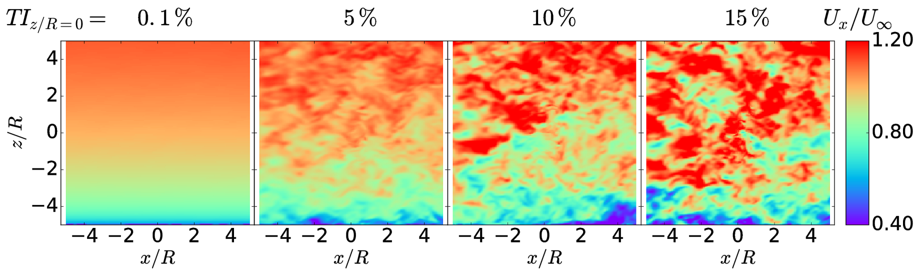

Figure 4. Vertical plane of instantaneous axial velocity component U_x in sheared flow for different longitudinal turbulence intensities $TI_{z/R=0}$ at hub position.

be deduced from experimental measurements if available. As they were not available for this experiment, standard conditions are assumed with $\alpha_p = 1/7$ (Pope, 2000).

2.3 Numerical framework

This work is realized within the open-source framework OpenFOAM[1] (version 2.2.2) together with the SOWFA[2] project, which contains a similar implementation of the ALM as presented by Troldborg (2009). A more detailed explanation of the implementation can be found in Martínez-Tossas et al. (2016). OpenFOAM is a set of libraries and executables entirely written in C++. While the first released scientific article about the framework was by Weller et al. (1998) its inner workings are described more in-depth by Jasak (1996).

The computational domain is cubic with an edge length of $L_x = L_y = L_z = 10\,R$ with R ~~as~~ the rotor radius and the rotor positioned at the domain center. The cells in the rotor vicinity are refined in the range of $-0.4 \leq x/R \leq 0.4$ with the size $\Delta x = D/128$. Within SOWFA several refinement zones are applied each time halving the cell edge length as also done in Vanella et al. (2008). The final mesh size consists of $1.9 \cdot 10^6$ cells. The technique used in SOWFA proves highly advantageous in terms of computational cost~~and its impact on the results are examined in a sensitivity study.~~. As the mesh dimensions at first sight seem relatively small compared to other work such as Troldborg (2009) or Martínez-Tossas et al. (2015b), an extensive sensitivity study was conducted by varying domain extents in axial direction up- and downstream of the rotor as well as in the lateral direction for different grid refinements. The findings show that the used dimensions have a negligible impact as shown in Nathan (2018).

For the boundary conditions the velocity is imposed as uniform inflow velocity of $\mathbf{U} = (U_\infty, 0, 0)$ for the non-turbulent flow and in the turbulent cases as the synthetic velocity as explained in section 2.2. The lateral boundaries are set as symmetric for

[1] OPENFOAM® (Open source Field Operation And Manipulation) is a registered trade mark of OpenCFD Limited, producer and distributor of the OpenFOAM software via wwww.openfoam.com.

[2] NWTC Design Codes (SOWFA (Simulator fOr Wind Farm Applications) by Matt Churchfield and Sang Lee) http://wind.nrel.gov/designcodes/simulators/SOWFA/. NWTC (National Wind Technology Center) is part of NREL (National Renewable Energy Laboratory) based in Golden, CO, USA.

the non-turbulent and homogeneous isotropic turbulence case. For the shear layer turbulence the velocity is also imposed at the lateral boundaries.

The large eddy simulations use the dynamic Lagrangian sub-grid scale model (Meneveau et al., 1996). For the discretization of the convective term a linear combination of 75% central differencing and 25% of a second-order upwind scheme is applied as presented by Warming and Beam (1976). In OpenFOAM terminology this scheme is called "Linear-upwind stabilized transport" (LUST). The choice of the scheme is made as a trade-off between the accuracy of a linear discretization and the stability of an up-winding scheme. This scheme proved to preserve well the turbulent structures (Nathan, 2018). The remaining spatial terms are discretized by central differencing and for the time discretization the Crank-Nicolson method is used.

The pressure is resolved using a geometric agglomerated algebraic multi-grid solver and the remaining variables are solved for with a bi-conjugate gradient method using a diagonal-based incomplete LU preconditioner. The total simulation run-time comprises 60 rotor revolutions ($\approx 8.5\,s$) and the time step has to be small enough to avoid the actuator point representing the blade tip skipping a computational cell during rotation. It is ~~also an integer fraction of the rotor revolution time. This~~ set at $0.327 \cdot 10^{-3}\,s$. The total run-time is chosen as first and second order statistics are deemed to be converged.

For the parametrization of the ALM, different distribution widths are chosen in order to obtain the optimum for the examined case and 40 actuator points are used to represent one blade in accordance with what was found in Nathan (2018).

3 Results

3.1 Validation and verification

The implementation was validated against EllipSys3D and verified against the MEXICO and NEW MEXICO experiment in Nathan et al. (2017). The MEXICO rotor is three bladed rotor with a radius $R = 2.25\,m$. It rotates at a constant RPM of $424.5\,min^{-1}$ for the three different flow cases with $U_\infty = \{10, 15, 24\}\,m/s$, hence their respective tip speed ratios are 10.0, 6.7 and 4.2. As shown in Nathan (2018), the chord based Reynolds numbers $Re = U_\infty c/\nu$ varies from $0.4 \cdot 10^6$ for the low velocity case towards the hub up to $0.6 \cdot 10^6$ for the high velocity case in the tip region. The power coefficients for the observed cases are $C_P = \{0.28, 0.36, 0.19\}$. A comparison of the axial profiles of the velocity components can be seen Figure (5) showing that both codes reproduce very similar results in the near wake further away from the rotor. ~~While the axial induction for $x/R \geq 0.5$ corresponds very well to the experimental data, the velocity deficit is under-predicted in the immediate rotor vicinity $-0.5 \leq x/R \leq 0.5$~~Apart for the high velocity case where 3D effects become important, an excellent agreement can be observed for the other two cases. For the high velocity case ($U_\infty = 24\,m/s$) the vortex sheets shed from the blades become visible by the oscillations in the axial velocity component U_x.

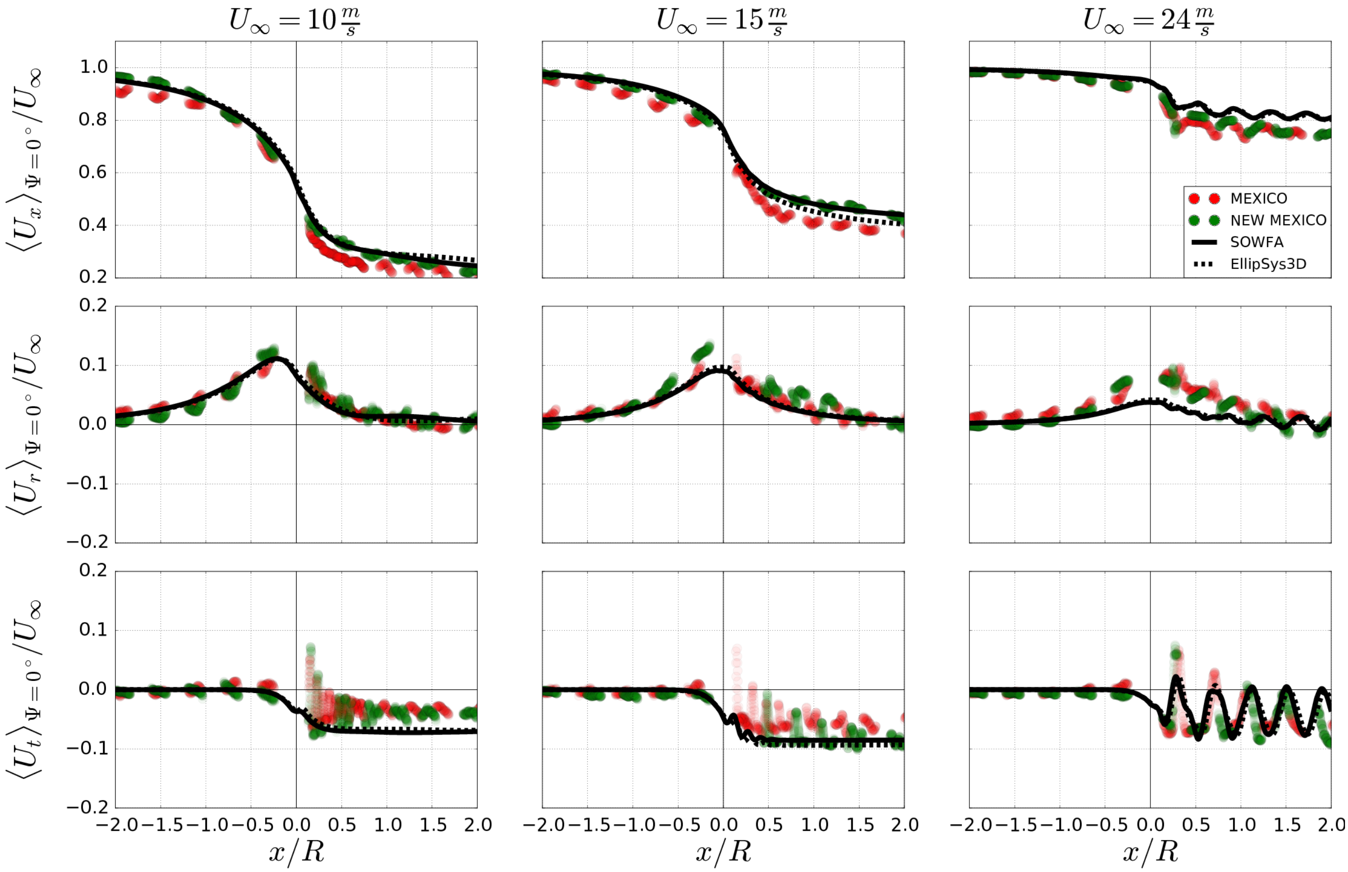

Figure 5. Axial profiles of phase averaged (rotor position $\Psi = 0^\text{o}$) velocity components ~~for~~ normalized by case specific reference velocity U_∞. Three different flow cases ~~an inboard and~~ for an outboard radial position are shown.

3.2 Non-turbulent flow

When refining the grid using the actuator line method the distribution parameter ϵ has to be adjusted to obtain a global torque $\langle T \rangle$ close to the reference value T_{ref}. In the following only the case for $U_\infty = 15\,m/s$ will be examined as the other cases in Nathan et al. (2017) served as extreme cases for determining how the model behaves at its limits.

Instead of relying on a constant $\epsilon/\Delta x$ for different grid resolutions, this work adapts $\epsilon/\Delta x$ depending on the grid resolution, or number of cells across the rotor diameter $N = 2R/\Delta x$. ~~This can be seen as a first step towards an actuator surface method, where the force is distributed with respect to the blades chord.~~ The results are shown in Figure (6). A confidence interval of $\pm 1\,\%$ was established around the reference torque value T_{ref}. Through iterations, an optimal distribution parameter is found to fall in this range.

The lower bound for the distribution parameter here is $\epsilon = 1.7\Delta x$ for the sake of numerical stability of the ~~here chosen~~ applied method. Other frameworks applying a different numerical discretization can go even lower ~~e.g.~~ *e.g.* in Ivanell et al.

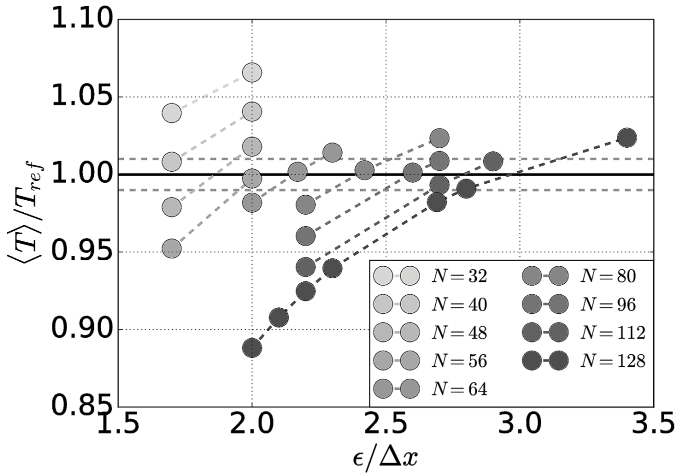

Figure 6. Relation between $\epsilon/\Delta x$ and resulting global torque normalized by reference torque for $U_\infty = 15\,m/s$.

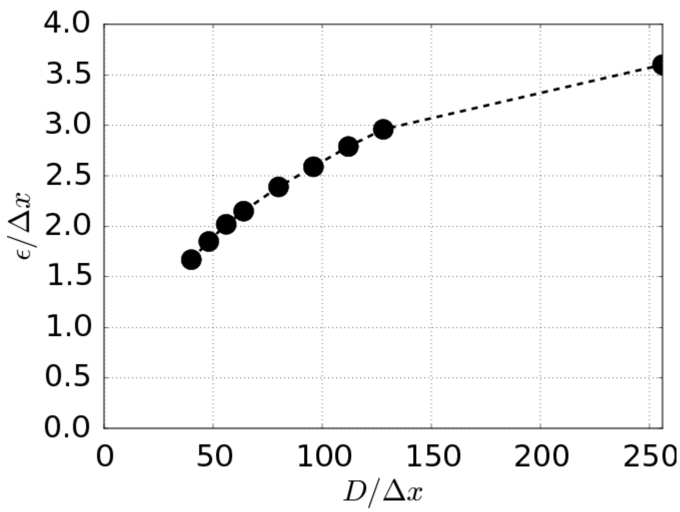

Figure 7. Optimal $\epsilon/\Delta x$ over number of cells for resolving one rotor diameter $D/\Delta x$.

(2010). By doing so it can be seen that the best solution in terms of global torque for a resolution of $N = D/\Delta x = 32$ is off by around 4% in Figure (6).

As a general trend it can be seen that $\epsilon/\Delta x$ has to be increased with increasing resolution. This stems from the fact that by refining the mesh with a constant $\epsilon/\Delta x$ the punctual induction caused by the blade would be too high and eventually the torque would be below the reference value, e.g. *e.g.* for $\epsilon = 2\Delta x$ for $N \geq 64$. On the contrary, when having a very low resolution a constant ϵ distributes the force too widely, causing a lower induction around the rotor resulting in an overestimation of the torque, e.g. *e.g.* for $\epsilon = 2\Delta x$ for $N \leq 48$.

The optimal distribution parameter $\epsilon/\Delta x$ found in Figure (6) are now shown in dependence of the grid resolution $N = D/\Delta x$ in Figure (7). It seems as if this value would reach eventually an asymptotic limit for higher resolutions. When looking at a more theoretical approach in Martínez-Tossas et al. (2015b) it is suggested that the optimal distribution width ϵ lies between $0.14 - 0.25$ of the chord c whereas in this case for $D/\Delta x = 128$ the ϵ/c lies between $0.5 - 8.9$ depending on the spanwise location. The observation made by Martínez-Tossas et al. (2015b) is backed by Shives and Crawford (2013) where ϵ/c falls in the same range. But it should be kept in mind that Shives and Crawford (2013) use a much higher grid resolution allowing $\epsilon/\Delta x \geq 4$ and in the case of Martínez-Tossas et al. (2015b) even $\epsilon/\Delta x \geq 5$.

The curvature in Figure (7) also confirms the findings of Jha et al. (2013) that keeping the relation $\epsilon/\Delta x = const$ while increasing the resolution is not a very good solution. While Ivanell et al. (2010) suggests to choose the smallest possible distribution width ϵ in order to minimize interactions with the vortical structures ($\epsilon/\Delta x = 1$), the observations made here fall more in line with work such as Shives and Crawford (2013) suggesting $\epsilon/\Delta x$ to be adapted to the physical model and in order to distribute the force over a meaningful length scale.

For an excerpt of the resolutions presented in Figure (6) the radial profiles of the velocity components can be found in Figure (8). It can be seen that the method seems to converge towards a solution when refining the mesh. As shown in Figure (6) the lowest resolution at $N = 32$ over-predicts the torque by distributing the force to widely which also reflects in the low axial induction downstream at $x/R = 0.13$. Despite following well the trend of the experimental values the method seems to converge towards radial profiles which are especially off in the tip and hub region where the strongest vortices are shed. These are limitations intrinsic of the ALM which is less apparent when using high fidelity approaches such as full rotor simulations (Carrión et al., 2015). In order to ameliorate the results at the tip, non-isotropic kernel could be investigated (Rullaud et al., 2018).

In Figure (9) the shed vortical structures can be seen in dependence on the grid resolution. While the root vortex is rather diffuse, a clear tip vortex can be noticed. It is interesting to notice the vortices shed around mid-span due to sub-optimal choice of the airfoils of blade causing a sudden change in circulation.

In order to estimate the resolution necessary to obtain tip vortex radii as seen in the MEXICO experiment the vortex radii are shown in Figure (10). The vortex radius r_{core} is defined as the limit containing 99% of the circulation. The Gaussian distribution is used as an approximation for the vorticity distribution within the vortex. This assumption is normally applied for low Reynolds number flows, while this case exhibits a Reynolds number of $Re = \Gamma/\nu = 220 \cdot 10^3$ $Re_\Gamma = \Gamma/\nu = 220 \cdot 10^3$. As these findings are related to the vortex dynamics of the flow Re_Γ is used instead of Re defined earlier. Nevertheless this

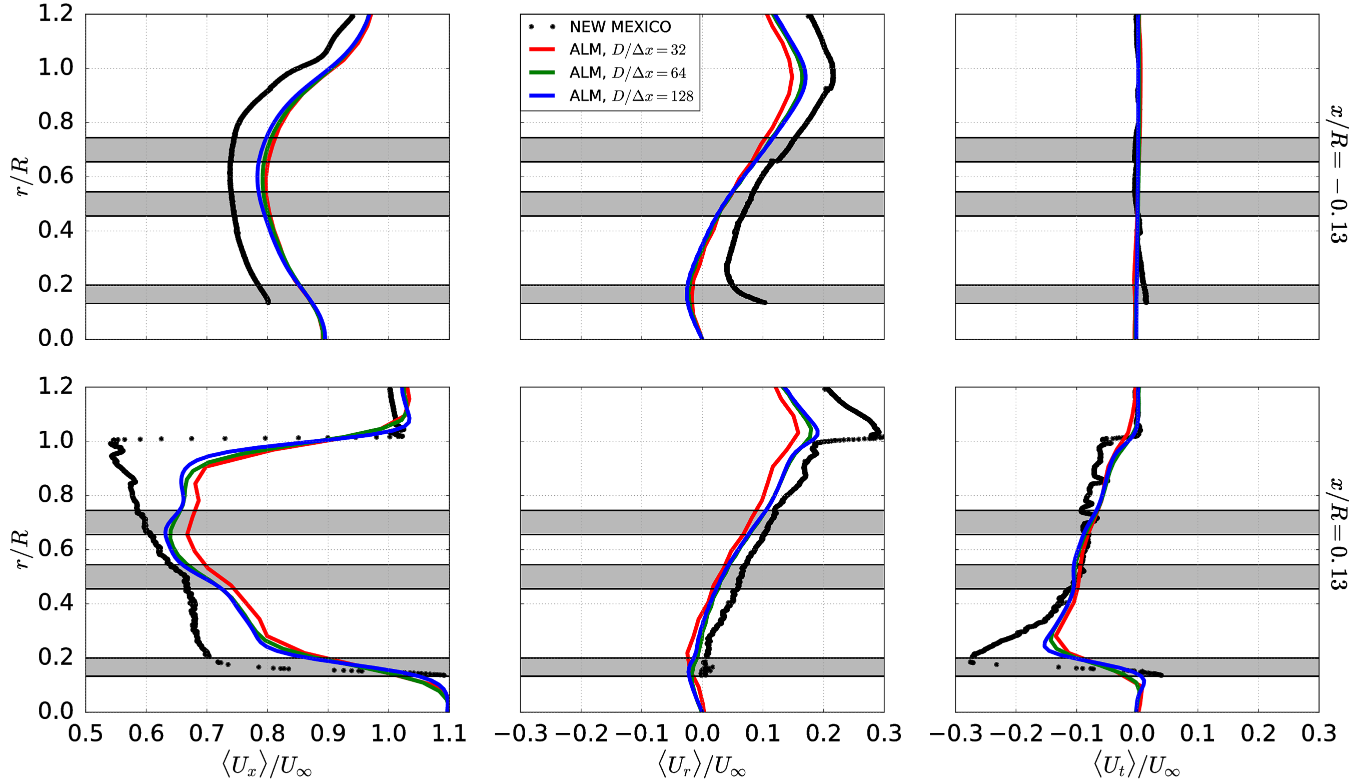

Figure 8. Radial profiles of time-averaged velocity components $\langle U_x \rangle$ (axial), $\langle U_r \rangle$ (radial) and $\langle U_t \rangle$ (tangential) for ALM in different grid resolutions at $x/R = 0.13$.

approximation is used in order to be able to draw an analogy between the experimental and the numerical results. It holds fairly well when comparing the Gaussian distribution and the vorticity for $N = 128$ as shown in Nathan (2018). Hence by assuming a Gaussian distribution for the vortices in the MEXICO experiment, a corresponding distribution parameter ϵ can be deduced as shown in Figure (10).

This would necessitate a resolution of $N \geq 4096$ for the ~~here~~ presented case which would result in a computational grid beyond any justifiable computational scope. Full rotor calculations as conducted by Carrión et al. (2015) allowed to obtain tip vortices of $r_{core}/R \approx 0.012$ for $N \approx 900$ in the tip region which corresponds very well to results in Figure (10). Another result for the vortex radius can be found in Nilsson et al. (2015) where for $\epsilon/\Delta x = 1$ and $N \approx 244$ in the tip region a vortex core radius of $r_{core}/R \approx 0.055$ was found. Despite the radii in this work and the references are calculated based on three different methods, the results fall within the same range.

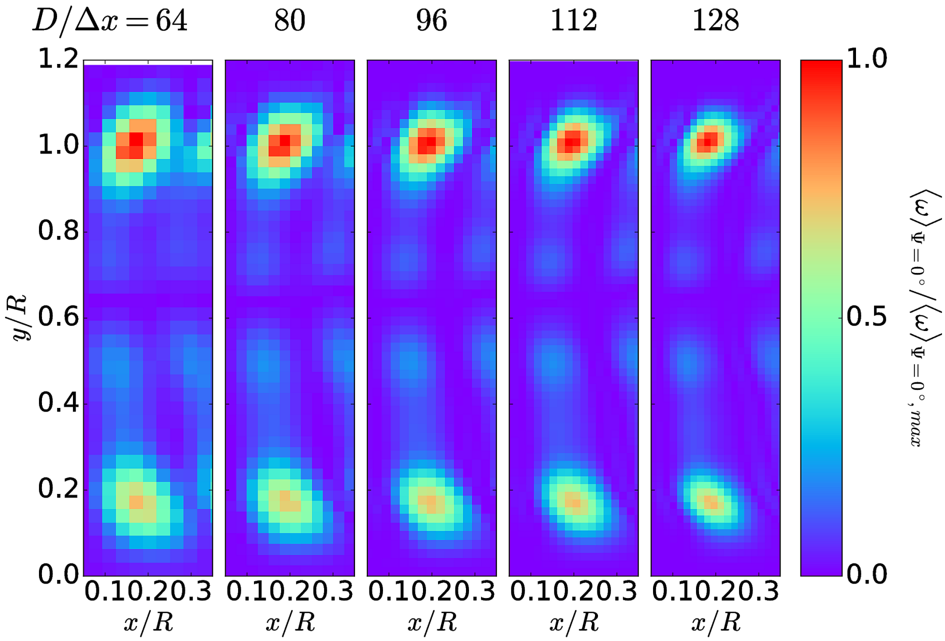

Figure 9. Normalized vorticity $\langle\omega\rangle_{\Psi=0^\circ}/\langle\omega\rangle_{\Psi=0^\circ,max}$ in the near wake for different grid resolutions.

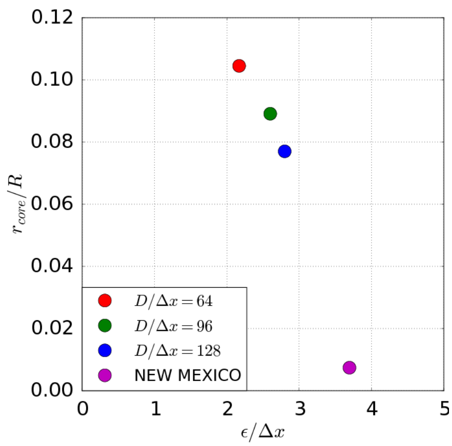

Figure 10. Normalized vortex radius r_{core}/R over normalized distribution parameter ~~ϵ/R~~ $\epsilon/\Delta x$.

3.3 Homogeneous isotropic turbulence

In Figure (11) the longitudinal evolution of the turbulence intensities can be seen. There is a stronger decay for higher turbulence intensities which was also found in Olivares Espinosa (2017). In that work EllipSys3D was compared to a solution based on OpenFOAM and it was found that over the same longitudinal distance of $10R$ ~~a decay~~ an absolute difference in the turbulence intensity of $48\,\%$ and $44\,\%$ occurred for each framework respectively. This stands in a stark contrast to the $4\,\%$ in this case for the high turbulence intensity case. This huge decay, which is even more significant for EllipSys3D, necessitates to approach the introduction of the turbulence close to the turbine for high turbulence intensity cases (Olivares Espinosa, 2017).

An important aspect when imposing a synthetic turbulence as boundary conditions of a CFD simulation is respecting the Nyquist–Shannon sampling theorem (Shannon, 1949) as also mentioned by Muller et al. (2014). Hence a study considering different ratios between the grid resolution of the synthetic turbulence and the simulation was undertaken. It is found that the higher the computational resolution is compared to the one of the synthetic turbulence, the less the turbulence intensity decays in longitudinal direction. While the criterion of Nyquist–Shannon states that the resolution of the computational domain should be ~~at least twice as big~~ $dx/\Delta x > 2$, this work uses the ratio of $dx/\Delta x = 2.5$ with dx ~~as~~ the cell width of the ~~synthetical~~ synthetic field and Δx ~~as~~ the cell width of the computational mesh.

When taking the case for $TI_{syn} = 5\,\%$ it is interesting to notice that while the resolved TI (green dashed line) is around $4.2\,\%$ at the rotor position $x/R = 0$ a huge part of the difference in relation to the imposed turbulence falls in the SGS model with $\langle TI_{res}\rangle + \langle TI_{sgs}\rangle = 4.8\,\%$ and finally just a relatively small amount of the turbulent intensity or turbulent kinetic energy is "lost" by numerical dissipation.

Despite the fact that the computational grid respects the Nyquist–Shannon criterion for signal sampling in respect to the synthetic grid, immediately at the inlet a part of the turbulence falls in the sub-grid range. Due to the numerical dissipation caused by the differencing schemes and turbulence modelling the energy cascade hands down its energy to lesser scales than the resolved ones.

It should be kept in mind, that the turbulence intensity the rotor model is experiencing through velocity sampling is the resolved turbulence intensity TI_{res} and the sub-grid turbulence intensity TI_{sgs} is therefore only felt indirectly, by an augmentation of the effective viscosity. When looking at the fraction of the resolved turbulent kinetic energy over the total turbulent kinetic energy, it can be seen that the resolved scales exceed $96\,\%$ which lies well above the criterion of $80\,\%$ proposed by Pope (2004). For the flow case with $U_\infty = 15\,m/s$ the total simulation runtime t_{tot} results in roughly $t_{tot} \cdot U_\infty/(10R) \approx 5.5$ flow through times. The synthetic turbulence field is large enough that it does not need to be recycled during one simulation.

In Figure (12) the effects of the ambient turbulence on the turbine wake are shown. While there are no ~~noticable~~ noticeable impacts for the low turbulence case with $TI_{syn} = 0.1\,\%$ the beginning of strong non-linear interactions can be observed for $TI_{syn} > 0.1\,\%$. For $TI_{syn} = 15\,\%$ the inflow turbulent structures seem to outgrow the structures created by the wind turbine.

In Figure (13) it can be seen how the strength of the vortical structures of the ambient fluid increases with higher turbulence intensity up-to the point for $T_{syn} = 15\,\%$ where its amplitude equals almost the one emitted by the rotor model. In Figure (14) the impact of the rotor presence on the energy spectrum can be seen. The wavenumber κ_p relating to the frequency of a blade

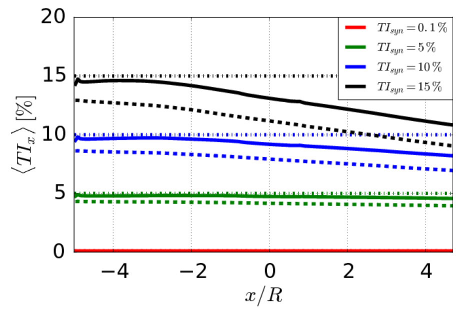

Figure 11. Longitudinal evolution of turbulence intensities for different turbulent intensities at the inlet in HIT without rotor effects. For each case the mean value $\langle TI \rangle$ is shown with the resolved TI $\langle TI_{res} \rangle$ (dashed line), resolved and subgrid scale TI $\langle TI_{res} \rangle + \langle TI_{sgs} \rangle$ (solid line) and the inlet TI TI_{syn} (dotted line) as reference. The sudden spike at the end of the domain is caused by the outlet condition and its influence is restricted to the last computational cell before the outlet.

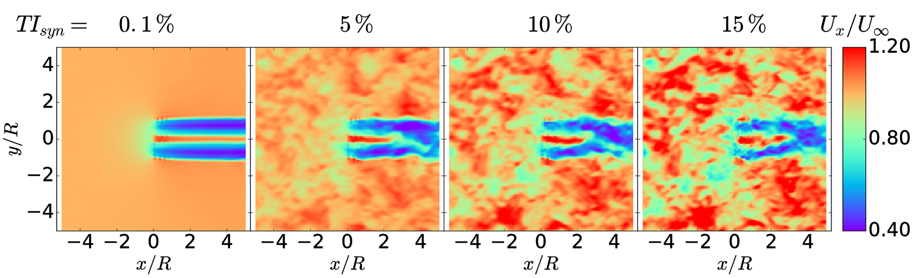

Figure 12. Instantaneous Normalized instantaneous axial velocity component U_x U_x/U_∞ of wind turbine wake immersed in HIT for different turbulence intensities.

passage (three times rotor frequency) obtained by $\kappa_p = 2\pi 3f/U_\infty$ shows a very distinct peak and its higher harmonics at the multiples of κ_p. As the velocity time series obtained from the simulations do not exhibit periodicity, the Welch method (Welch, 1967) is used to generate the energy spectra.

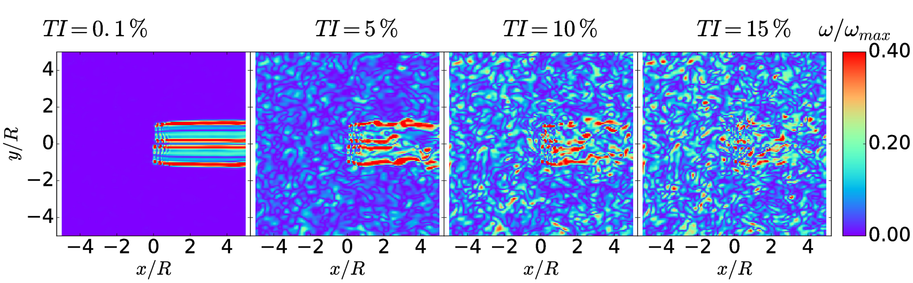

Figure 13. Instantaneous Normalized instantaneous vorticity fields ω_x/ω_{max} of wind turbine wake immersed in HIT for different turbulence intensities.

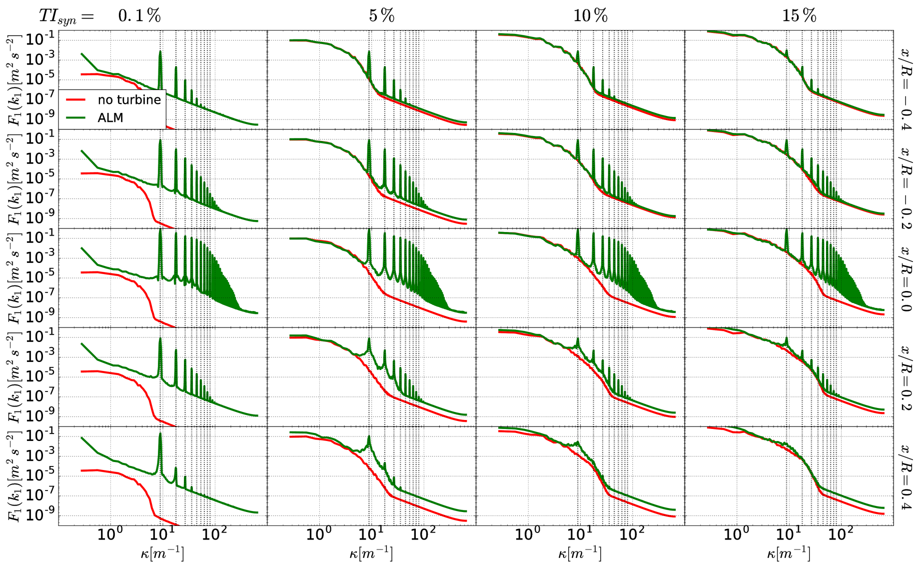

Figure 14. Impact The energy spectra for the HIT based on the time-series of the axial velocity component at different points in the near wake ($x/R = \{-0.4, -0.2, 0, 0.2, 0.4\}$) for different inlet turbulent intensities $T_{syn} = \{0.1, 5, 10, 15\}\,\%$ are shown. The impact of the rotor presence on energy spectrum with can be seen by the spikes at the wavenumber relating to 3 times the rotor frequency and its higher harmonics indicated by (dotted black lines. Each column represents the different turbulence intensity cases and the rows are representing different axial positions of the spectra).

It is interesting to notice the distinct peaks in the spectra occur at the wavenumber relating to the frequency of the blade passage and its harmonics. The harmonics are caused by the strong excitement of the fluid by the blade passage and its interaction with the non-linear term in the NS equations. As the blade forces and hence the strength of the tip vortices are very comparable, the peaks are very similar among the different cases for $-0.4 \leq x/R \leq 0.2$. The higher the turbulent kinetic energy content stemming from the ambient flow the faster the peaks are dampened and blend into the ambient flow. For example there is almost no discernible effect by the blade at $x/R = 0.4$ for $TI_{syn} = 15\,\%$ while for $TI_{syn} = 0.1\,\%$ the velocity oscillations are still very noticeablenoticeable. Although it is of lesser amplitude also the upstream region is under the influence of the distinct blades up-to a certain extent.

3.4 Shear layer turbulence

The instantaneous and mean velocity fields with an immersed rotor can be seen in Figure (**??**). The horizontal plane at hub height again seems to behave similar to the HIT cases in Figure (12). When looking at the vertical planes in Figure (15) the influence of the sheared flow can be seen by a higher velocity deficit in the wake on the lower half of the rotor. Horizontal plane of instantaneous axial velocity component U_x of wind turbine wake immersed in shear turbulent flow at hub height.

When looking at the instantaneous normalized vorticity in Figure (**??**) it can be seen that while the vortical structures emitted by the rotor are prevalent for low turbulence intensity cases, they seem to get even for $TI_{x,z/R=0} \geq 10\,\%$. Hence the turbulent

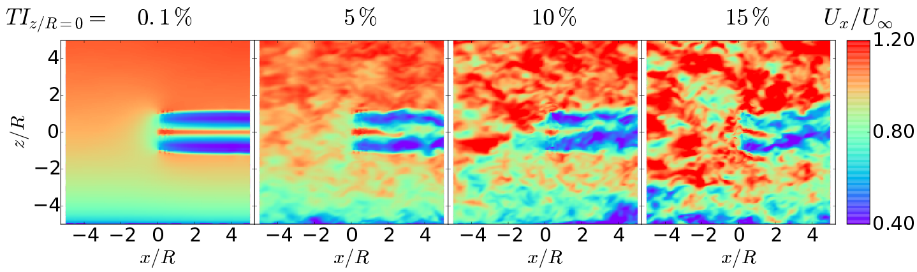

Figure 15. Vertical plane of instantaneous axial velocity component U_x of wind turbine wake immersed in shear turbulent flow.

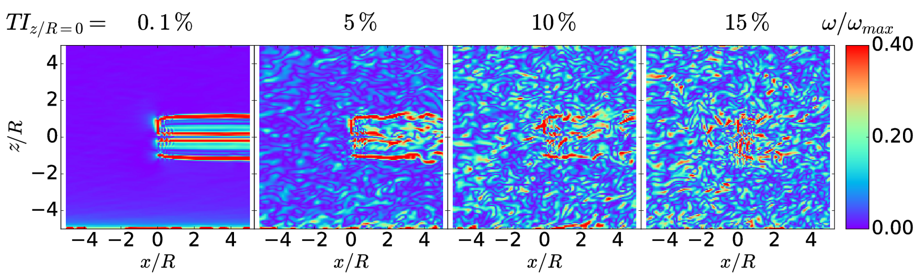

Figure 16. Instantaneous normalized vorticity ω/ω_{max} in sheared flow for different longitudinal turbulence intensities TI_x at hub position. vertical plane at $y/R = 0$

~~structures of the ambient flow become as significant as the ones emitted from the wind turbine. This is of particular interest for estimating the range up-to which the effects of the distinct blades can be felt which serves often as a measurement for determining the near wake.~~ WIn the vertical plane in Figure (16) it can be seen that there is an increase in the vorticity magnitude towards the ground. ~~Instantaneous normalized vorticity ω/ω_{max} in sheared flow for different longitudinal turbulence intensities TI_x at hub position. horizontal plane at $z/R = 0$~~ While the increase appears to be rather subtle, it is shown in Nathan (2018) that the TI increases significantly towards the ground as expected in a shear layer flow.

Looking at the energy spectra in Figure (17) ~~reveal~~ reveals a similar picture as shown above for the case of homogeneous isotropic turbulence. As the blade forces and hence the strength of the tip vortices are very comparable, the peaks are very similar among the different cases for $-0.4 \leq x/R \leq 0.2$. Due to the dissipation caused by the ambient turbulence these peaks dampen at a different pace as seen at $x/R = 0.4$.

While before and at the rotor position for $-0.4 \leq x/R \leq 0$ the peaks remain very distinct, vortical structures by the ambient fluid and emitted by the blade cause the injected peaks to dampen and distributing energy to adjacent wavenumbers as seen clearly for $x/R \geq 0.2$. Depending on the level of the ambient turbulence the peak gets attenuated up-to a point where it blends almost completely in with ambient turbulence as seen for $TI_{x,z/R=0} = 15\%$ at $x/R = 0.4$. This relates to the observation made earlier ~~when looking at Figure (??) and Figure (??) where the~~ that ambient structures are almost as important as the structures emitted by the blade.

Spectra of different axial positions at hub height z/R for the shear layer turbulence case. Each column represents the different turbulence intensity cases and the rows are representing different axial positions of the spectra.

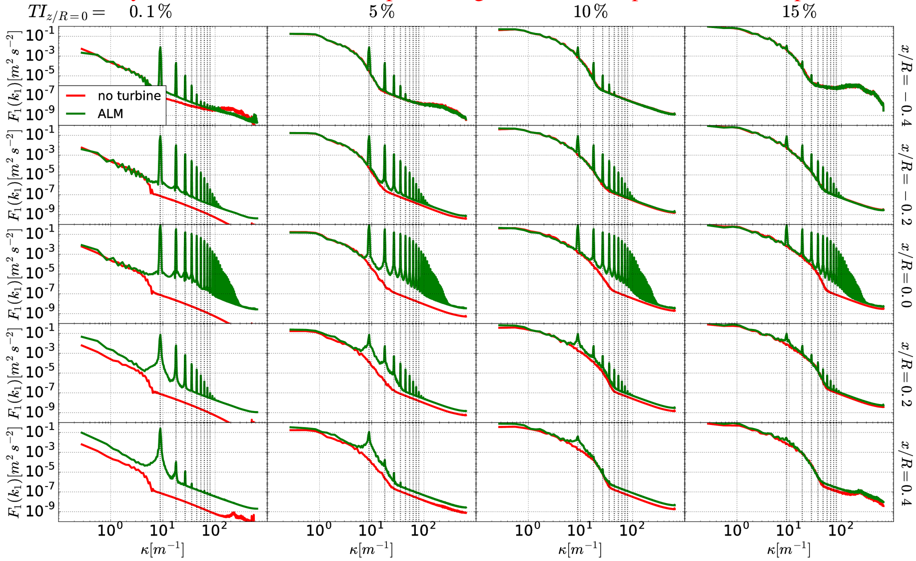

Figure 17. The energy spectra for the shear layer flow based on the time-series of the axial velocity component at different points in the near wake ($x/R=\{-0.4,-0.2,0,0.2,0.4\}$) for different inlet turbulent intensities $T_{syn}=\{0.1,5,10,15\}\,\%$ at hub height $z/R=0.0$ are shown. The impact of the rotor presence can be seen by the spikes at the wavenumber 3 times the rotor frequency and its higher harmonics (dotted black lines).

This is particularly interesting for examining the reach of the here used rotor model and the distinct presence of the separate blade forces. It seems that for a realistic case with a turbulent shear flow and a means that the near wake in a turbulent flow with an ambient turbulence intensity of $TI_{x,z/R=0} \geq 10\,\%$ the velocity fluctuations at $x/R=0.4$ already seem to have only a weak relation to the injected turbulence by the rotor but a much stronger one to the ambient turbulence. This means that for this kind of flow probably a actuator disk method would also be sufficient when looking at the flow characteristics beyond $x/R=0.4$.

Although flow properties were maintained at a similar level, the sheared flow has a clear impact on the power extraction and also on vortex properties of the structures emitted by the blade. A very interesting observation is the fact that for higher turbulence intensities the effects of the distinct blades using the ALM seems to vanish at relatively short downstream distances. This poses the question of the usability of the ALM when arguing for its capabilities of representing the transient behaviour and its impact on downstream turbines.

4 Conclusions

By using a validated actuator line implementation (Nathan et al., 2017), it was shown that the distribution width $\epsilon/\Delta x$ has a non-linear dependence on the grid resolution and converges probably towards values suggested in Martínez-Tossas et al.

(2016). The rotor torque is used as a global indicator for determining the distribution width, but the rotor thrust followed the same trend. Hence it is interesting to see that while the rotor induction is predicted well, the velocity deficit agrees well only for $x/R > 5$ but not in the ultimate rotor vicinity.

It is also shown that with increasing grid resolution the spatial profiles seem to converge. This would be one aspect of a grid independent solution, but it is still very far away from resolving correctly the shed tip vortices. Although it seems to converge towards a value of $\epsilon/\Delta x \approx 4-5$ for which the dimensions of the experimental vortices would be attained, this causes excessive computational costs due to the large mesh.

When looking at the turbulent inflow, a synthetic turbulence generated by the Mann algorithm (Mann, 1998), it was shown that the decay of the turbulence intensity in longitudinal direction is much less pronounced than in previous work. As shown for the axial decay of the turbulence intensity a significant part of the difference between the resolved turbulence intensity and the imposed one from the synthetic field, resides within the sub-grid scales. Hence there is very little loss due to numerical dissipation which also reflects in the energy spectra which are the better the higher the turbulent content is.

As expected the wake does recover at a faster pace for a higher turbulence intensity. It is very interesting to notice that the turbulent structures of the ambient flow eventually catch up with the amplitude of the structures emitted by the rotor. This is already ~~noticable~~ noticeable in the instantaneous velocity fields but becomes even clearer when evaluating the spectra. When considering the velocity fluctuations in the downstream flow caused by the blade passages for determining the near wake, it can be observed that in this case for $TI_{syn} \geq 10\,\%$ the near wake already ends at $x/R = 0.4$. This is particular interesting as a turbulence intensity of $15\,\%$ at hub height is still considered to be low turbulence intensity according to ISO 61400 and many real sites exhibit even higher turbulence intensities. Hence for some cases the limit of the near wake would be $x/R = 0.4$ and even lower.

Code and data availability. The SOWFA framework on which this work is based is made available by NREL https://github.com/NREL/SOWFA/ and the turbulence generator for the homogeneous isotropic turbulence can be obtained via http://vbn.aau.dk/en/publications/tugen(3e097a90-b3d8-11de-a179-000ea68e967b).html. The results for the NEW MEXICO experiments were provided upon request by Gerard Schepers.

Competing interests. Christian Masson is a member of the editorial board of the journal.

Acknowledgements. This work is partially supported the Canadian Research Chair on the Nordic Environment Aerodynamics of Wind Turbines and the Natural Sciences and Engineering Research Council (NSERC) of Canada. Thanks for the great work done by Matthew Churchfield and colleagues at National Wind Technology Center, Boulder, CO, by establishing the open source framework SOWFA. The data used have been supplied by the consortium which carried out the EU FP5 project Mexico: 'Model rotor EXperiments In COntrolled conditions'. Thanks also a lot to Gerard Schepers for providing results of the NEW MEXICO experiment.

References

Carrión, M., Steijl, R., Woodgate, M., Barakos, G., Munduate, X., and Gomez-Iradi, S.: Computational fluid dynamics analysis of the wake behind the MEXICO rotor in axial flow conditions, Wind Energy, 18, 1023–1045, 2015.

Gilling, L.: TuGen, Tech. rep., Department of Civil Engineering, Aalborg University, 2009.

Glauert, H.: Airplane Propellers, in: Aerodynamic Theory, Vol. IV, Division L, edited by Durand, W. F., pp. 169–360, Springer, New York, 1935.

ISO 61400: Wind turbines, 2015.

Ivanell, S., Mikkelsen, R. F., Sørensen, J. N., and Henningson, D.: Stability analysis of the tip vortices of a wind turbine, Wind Energy, 13, 705–715, 2010.

Jasak, H.: Error analysis and estimation for finite volume method with applications to fluid flow, Ph.D. thesis, Imperial College, 1996.

Jha, P. K., Churchfield, M. J., Moriarty, P. J., and Schmitz, S.: Guidelines for Actuator Line Modeling of Wind Turbines on Large-Eddy Simulation-type Grids, Journal of Solar Energy Engineering, 136, 1–11, https://doi.org/10.1115/1.4026252, 2013.

Krogstad, P.-Å. and Eriksen, P. E.: "Blind test" calculations of the performance and wake development for a model wind turbine, Renewable Energy, 50, 325–333, https://doi.org/10.1016/j.renene.2012.06.044, 2013.

Mann, J.: Wind field simulation, Probabilistic Engineering Mechanics, 13, 269–282, https://doi.org/10.1016/S0266-8920(97)00036-2, 1998.

Manwell, J., McGowan, J., and Rogers, A.: Wind Energy Explained: Theory, Design and Application, Wiley, 2010.

Martínez-Tossas, L. A., Churchfield, M. J., and Leonardi, S.: Large eddy simulations of the flow past wind turbines: actuator line and disk modeling, Wind Energy, 18, 1047–1060, 2015a.

Martínez-Tossas, L. A., Churchfield, M. J., and Meneveau, C.: Optimal smoothing length scale for actuator line models of wind turbine blades, Wind Energy, 00, 1–14, 2015b.

Martínez-Tossas, L. A., Churchfield, M. J., and Meneveau, C.: A Highly Resolved Large-Eddy Simulation of a Wind Turbine using an Actuator Line Model with Optimal Body Force Projection, Journal of Physics: Conference Series, 753, 082 014, 2016.

Meneveau, C., Lund, T. S., and Cabot, W. H.: A Lagrangian dynamic subgrid-scale model of turbulence, Journal of Fluid Mechanics, 319, 353, https://doi.org/10.1017/S0022112096007379, 1996.

Muller, Y.-A., Masson, C., and Aubrun, S.: Large Eddy Simulation of the meandering of a wind turbine wake with stochastically generated boundary conditions, Journal of Physics: Conference Series, 524, 012 149, 2014.

Nathan, J.: Application of the actuator surface concept in large-eddy simulations with regards to the near wake of wind turbines, Ph.D. thesis, ÉTS Montréal, 2018.

Nathan, J., Forsting, A. R. M., Troldborg, N., and Masson, C.: Comparison of OpenFOAM and EllipSys3D actuator line methods with (NEW) MEXICO results, Journal of Physics: Conference Series, 854, 012 033, 2017.

Nilsson, K., Shen, W. Z., Sørensen, J. N., Breton, S.-P., and Ivanell, S.: Validation of the actuator line method using near wake measurements of the MEXICO rotor, Wind Energy, 18, 499–514, 2015.

Olivares Espinosa, H.: Turbulence Modelling in Wind Turbine Wakes, Ph.D. thesis, ÉTS Montréal, 2017.

Pope, S.: Turbulent Flows, Cambridge University Press, 2000.

Pope, S. B.: Ten questions concerning the large-eddy simulation of turbulent flows, New Journal of Physics, 6, 1–24, https://doi.org/10.1088/1367-2630/6/1/035, 2004.

Rullaud, S., Blondel, F., and Cathelain, M.: Actuator-Line Model in a Lattice Boltzmann Framework for Wind Turbine Simulations, Journal of Physics: Conference Series, 1037, 022 023, http://stacks.iop.org/1742-6596/1037/i=2/a=022023, 2018.

Sanderse, B., van der Pijl, S., and Koren, B.: Review of computational fluid dynamics for wind turbine wake aerodynamics, Wind Energy, 14, 799–819, 2011.

Sarmast, S., Segalini, A., Mikkelsen, R. F., and Ivanell, S.: Comparison of the near-wake between actuator-line simulations and a simplified vortex model of a horizontal-axis wind turbine, Wind Energy, 19, 471–481, 2016.

Schepers, J., Boorsma, K., Cho, T., Gomez-Iradi, S., Schaffarczyk, P., Jeromin, A., Shen, W., Lutz, T., Meister, K., Stoevesandt, B., Schreck, S., Micallef, D., Pereira, R., Sant, T., Madsen, H., and Sørensen, N.: Final report of IEA Task 29, Mexnext (Phase 1): Analysis of Mexico wind tunnel measurements, Tech. rep., ECN, 2012.

Shannon, C. E.: Communication in the presence of noise, Proceedings of the IRE, 37, 10–21, 1949.

Shen, W. Z., Zhu, W. J., and Sørensen, J. N.: Actuator line/Navier–Stokes computations for the MEXICO rotor: comparison with detailed measurements, Wind Energy, 15, 811–825, 2012.

Shives, M. and Crawford, C.: Mesh and load distribution requirements for actuator line CFD simulations, Wind Energy, 16, 1183–1196, 2013.

Troldborg, N.: Actuator Line Modeling of Wind Turbine Wakes, Ph.D. thesis, DTU, Copenhagen, DK, 2009.

Troldborg, N., Larsen, G. C., Madsen, H. A., Hansen, K. S., Sørensen, J. N., and Mikkelsen, R. F.: Numerical simulations of wake interaction between two wind turbines at various infl ow conditions, Wind Energy, 14, 859–876, 2011.

Vanella, M., Piomelli, U., and Balaras, E.: Effect of grid discontinuities on large-eddy simulation statistics and flow fields, Journal of Turbulence, 9, 37–41, https://doi.org/10.1080/14685240802446737, 2008.

Vermeer, L. J., Sørensen, J. N., and Crespo, A.: Wind turbine wake aerodynamics, Progress in Aerospace Sciences, 39, 467–510, https://doi.org/10.1016/S0376-0421(03)00078-2, 2003.

Warming, R. and Beam, R. M.: Upwind second-order difference schemes and applications in aerodynamic flows, AIAA J, 14, 1241–1249, 1976.

Welch, P. D.: The Use of Fast Fourier Transform for the Estimation of Power Spectra: A Method Based on Time Averaging Over Short, Modified Periodograms, IEEE Transactions on Audio and Electroacoustics, 15, 70–73, https://doi.org/10.1109/TAU.1967.1161901, 1967.

Weller, H. G., Tabor, G., Jasak, H., and Fureby, C.: A tensorial approach to computational continuum mechanics using object-oriented techniques, Computers in Physics, 12, 620–631, https://doi.org/10.1063/1.168744, 1998.

Anonymous Referee #1

General remarks:

This paper is of overall very good quality. A detailed discussion on the impact of the actuator line parameters is given. Even so no generic solutions are given, some metrics can be extracted from the work, regarding the optimal values of the Gaussian width parameter. Based on this validated actuator-line model, the authors propose a study on the impact of a homogeneous, isotropic turbulent inlet and shear layer turbulence. While the impact of the homogeneous isotropic turbulence is clear and well exposed thanks to the provided spectra, the additional impact of the shear layer is less obvious and should be discussed in more details.

Specific comments:

- P3 L9. Airfoil polars as a function of the Reynolds number are not given in Schepers et al. Please clarify.

See P3, L9, Shen 2012 is taken as reference.

- P3 L12. The root correction by Shen is mentioned, but supposed to have "known outcome". Is it possible to clarify? Furthermore, other corrections have been proposed in the literature (see Snel, Chaviaropoulos, Bak, Dumitrescu. . .). Is it possible to include them?

At this point, it is difficult to include them. I removed controversal "known outcome".

- P3 L12. Coriolis / Centrifugal forcing enhance the lift of the airfoil near the root of the blade, not over the whole blade. It should be clearly stated here.

Done, see P3L11.

- P3 L12. It is disappointing to see that purely 2D airfoil polars are used, while 3D effects are discussed.

It was shown in Nathan 2017, that it is more than sufficient for the 15 m/s case.

- P3 L16 → P4 L3. The authors argue the Glauert tip correction should be used due to the low resolution. According to Churchfield et al. (2017), this is due to the isotropic kernel that is used, and the virtual projection of forces outside of the "blade domain". It could be interesting to see which phenomena is dominating, i.e. the lower resolution or the isotropic projection. Furthermore, I was not able to find reference (Nathan, 2018). Is it already published? Otherwise, please mention it in the references.

It would definitely be interesting, but it would be the matter of future work. Nathan, 2018 references to my PhD thesis, which should already be available since a while in a digital form at the library of ETS. I am in contact with the school in order to find out, why this has yet happened. I handed it in more than 6 months ago.

- P6 L7. The domain is rather small in length compared with standard recommendations. As a comparison, N. Troldborg (2009) uses a domain length of 18R, MartinezTossas (2015) use a domain length of 21D. . . It could be useful to provide some proof of convergence.

A complete sensitivity study was conducted in my PhD thesis. Including the numerous graphics and tables would blow up this article unnecessarily.

- P6 L25. If possible, provide some orders of magnitude for the time step.

Done, see P7L4.

- P7 L6. The under-prediction of the axial induction is not clear to me; results are almost super-imposed to the NewMexico measurements. C2

True, I rephrased that passage.

- P8 L5 → L7. I do not understand the link with the actuator surface method. Even so epsilon over dx is adapted, depending on the Cartesian grid refinement, it is still an actuator line, and no chord-wise meshing is used.

I agree, it is still an ALM, passage adapted.

- P8 L14 → 18. Discussion regarding the impact of the epsilon parameter is very instructive. Giving a look at the results, it seems to me there is an almost linear relation between the optimal epsilon value (leading to T/T_{ref} = 1) and the mesh refinement parameter N in the range 50 < N < 150. It could be interesting to derive an empirical law from it. In case the results presented in Figure 6 are not "rotor specific", this could lead to a very simple law to derive the value of epsilon "on the fly".

I share your enthusiasm on this. Probably this method should also be applied to e.g. NTNU blind comparison test or other experiments and see whether an empiricial relation could be derived. In my opinion it is slightly non-linear as seen in Fig.7.

- P9 L13→L16. The "bad" resolution near the tip is, according to the authors, attributed to the actuator-line representation of the blades. In Blondel et al. 2017, a lifting-line model is used together with a vortex model of the wake, and better correlation with experimental data was obtained (compared to SOWFA simulations). Thus, from my point of view, discrepancies should be attributed to the isotropic kernel in use, which is unrealistic near the tip, or the potential excessive diffusion of the finite volume scheme. The effect of the isotropic Gaussian kernel and the mesh effects, as discussed P10., should be further analyzed (not necessarily in this publication, as this is not the main topic).

I agree, I think it goes in hand with your point mentioned above and a possibility for future work.

- P12. In this part, synthetic turbulence is imposed at the inlet of the domain. I guess results presented in Figure 11 are based on simulations without the wind turbines, considering only the evolution of the TI in a channel. A net decrease of the turbulence intensity is observed along the channel. The simulations are not really described here. It could be interesting to provide some proof of convergence. Is the simulation time long enough to transport the characteristics defined at the inlet? This could be a basic explanation to the decrease of the TI that is observed. Also, it seems something is happening at the outlet, with some kind of sharp TI recovery. If this belongs to ghost cells, it should not be present in this plot. The effect of the ratio between the CFD grid and the SEM grid is discussed. One can wonder about the turbulent length scales used C3 in the SEM algorithm, and their relation with the size of the computational grid. Is the CFD grid fine enough to catch the vortices given at the inlet?

Yes, the numerical grid cell size was chosen to respect the Nyquist-Shannon criterium, hence it was more than twice as refined as the synthetical grid.

- P14. Figure 15 is not useful and could be removed. Same remark holds for Figure 17, results are similar to the homogeneous isotropic turbulence case.

Done, removed.

- P15. In 2.2.2., the evolution of mean velocity with height is presented. However, is seems to me, based on the contours of vorticity, that the TI is constant with height. Is that correct? From a physical point of view, higher TI is expected near the ground. This should lead to higher vorticity. Can the author provide some insight? In figure, y label should be z/R.

Passage adapted, TI changes with height, but you are right, it is rather hard to notice with the vorticity plots.

- P16. L7. I do not understand the point here. Please reformulate.

Done, reformulated.

- P16. L11. Are the authors talking about the global rotor power? No metrics are given. The impact on vortex structures is not clear to me. Differences in the spectra between figure 19 and 14 are rather small. I would suggest including an additional metrics here to clarify the impact of the shear on the near wake.

Passage removed. It is discussed more in detail in my thesis, but it does not necessarily has to be in the article.

- P17. Conclusions. Based on the observation of the turbulence decay (fig. 11) with axial position, it seems that at high TI, a large part of the TI is included in the subgrid scales. Therefore, I am not totally comfortable with the conclusions that are given: the length of the near-wake is determined based on the observation of the vorticity. However, the subgrid-scales are not included in the vorticity. Therefore, it seems difficult to draw definitive conclusions. As a more general remark, this work emphasize on the impact of the TI on the near-wake. However, blade loads may also be impacted, even at the airfoil polar level. One might expect a delay in the stall at high TI, which could impact the blade root loads. Also, it could have been interesting to use the NTNU Blind Comparison experiments as a complementary validation case.

True, I think it is a shortcoming of my work, that I did not have the time to conduct this experiment with another rotor. It is true, that some of the turbulent motion falls within the subgrid, but as shown in my PhD thesis, more than 90% fall within the resolved scales. Hence I only take the resolved scales into consideration when looking at the limits of the near wake.

Technical corrections:

- P1 L2. Noticable → Noticeable C4

Done.

- P1 L3. This works uses → This work uses

Done.

- P1 L24. To to assess → To assess

Done.

- P2 L12. “As done the former approach”

Done.

- P2 L29. Change “as the . . .” → With F representing. . . U the. . . (etc).

Done.

- P2 L32. Reformulate. “Finally, a summary is given. . .”

Done.

- P3 L8 Gaussian Kernel G → G the Gaussian Kernel

Done.

- P3 L8 Parenthesis: (f_{tip} → f_{tip}

Done.

- P3 L10 This data → These (plural)

Done.

- P4 L14. Latin abbreviations should be in italic (e.g.)

Done.

- P4 L15. Acronym HIT has never been defined - P8 L6. .This can. . . (missing space)

Done.

- P8 L10. “here chosen method” (reformulate)

Done.

- P8 L16. E.g. → Italic

Done.

Anonymous Referee #2

The manuscript entitled "Near wake analysis of actuator line method immersed in turbulent flow using large-eddy simulations" deals with numerical computations of a modelled wind turbine embedded in LES computations. Several types of inflow turbulence are implemented in order to study its effect on the near wake development. The spectral content of the wake flow is then used as indicator of modifications. The present study is of interest for the wind energy community ad gives valuable insights on the near wake extent depending on turbulence intensities and types. On the other hand, the manuscript needs several improvements before to be accepted for publications.

- In general, the figure captions are poor and lack of essential information.
Discussion paper should be able to understand the figure content just be reading the caption. Some axes are wrong. Some figures are not consistent with each other

Several figure captions and figures were redone.

- The manuscript should be self-consistent. Please remind the main parameters of the MEXICO / NEW MEXICO experiments: rotor dimensions, tip speed ratio, hub size, Reynolds number based on chord length, etc.

Added, see P7L10-15.

- What are the properties of the generated turbulence in term s of scales: integral length scale, ratio between this scale and the rotor radius? Since the authors present some turbulence spectra without wind turbines, it would be worth to develop a better description of the generated turbulence.

Added length scale of incoming turbulence P5L9, R/4.

- The PhD thesis of the 1st author is cited regularly, whereas the reference is not precise enough to ensure that the reader will find it easily on the web. Additionally, this reference is sometimes cited for results which are not specifically a new outcome of this thesis. So please cite more relevant sources when possible.

Nathan, 2018 references to my PhD thesis, which should already be available since a while in a digital form at the library of ETS. I am in contact with the school in order to find out, why this has yet happened. I handed it in more than 6 months ago.

Major comments:

- P2, lines 22-24: the spectra are also based on statistics. I do not see why it would be less sensitive than second-order statistics to the convergence issue, since the spectra is a frequency distribution of the variance.

In wavenumber space it is easier to detect at which point the structures emitted from the blade merge with the surrounding turbulence. Also time series for energy spectra were taken at different points at the circonference of the rotor. Hence the spatial aspect can be neglected and it the energy spectra for each point can be averaged and the result is a smoother energy spectrum. This would not be possible with a radial profile of TI due to the asymmetric nature of the helicoidal vortical structures.

- P3, line 10-12 : this data was obtained from wind tunnel experiments and therefore it does not include the stall delay due to boundary layer stabilizing effects such a Coriolis and centrifugal forcing which enhance the lift of the airfoil". These types of effects can be reproduced in a wind tunnel. Do you mean 2D experiment? Without rotation?

Yes, passage was adapted.

- Page 5, lines 4-6. Give some details about the synthetic turbulence fields: what are the turbulent length scales ? it seems that the turbulence does not dissipate with the axial distance. That is not so common, as explained later on in the manuscript. Some comments should be already mentioned here.

Added, P5L9. It does dissipate, see Fig. 11, but at a lower pace than in other work.

- Figure 5 : improve the caption and give details about the experimental configuration used as reference here : power coefficient, thrust coefficient, TSR, etc

Done, P7L10-15.

- Page 10, line 15-17 : this part is confusing : it seems that a relative decrease of turbulence is given (48% and 44%), whereas the 4% stands for a decrease of turbulence from 15% to 11%. This would correspond to a relative decrease of 25%... please rephrase this part.

Done, rephrased.

- Page 16, lines 11-15. Please elaborate more on the discrepancies between sheared and un-sheared conditions

Removed passage.

- Conclusion: there is not discussion about the relative size of the inflow turbulent structures compared to the wake turbulent structures (rotor size, blade size, tip vortex size, shear layer size?). It is indeed a very important parameter to justify the observations mentioned in page 17, lines 16-23. Minor comments:

Done, P7L10-15.

- P1, l24 : "to to"

Done.

- Figure 2 : if it the midplane at y/R = 0, the plot should be dependant of z/R and x/R

Done.

- P3, line 8 : one parenthesis is missing - P4, line 2 : "Kernel function"

Done.

- P4, line 3: please give the definition of sigma and Delta x.

Done.

- Figure 8 is too small. Additionally, it is difficult to differentiate the experimental and numerical results

Done.

- Page 10, line 2: The Reynolds number is based on the circulation: Please explain why you use this definition and not another one.

Done, see P10L10-12.

- Pge 10, line 7 : remove “here”

Done.

- Figure 10 : the caption is wrong

Done.

- Figure 11: the caption is poor and the authors should also better explain in the body text what this figure is for. Which computation solver is used here?

Done.

- Page 12, line 8 : “. . . should be at least twice as big” means dx/Delta x >2 ?.

Done.

- Figures 12 and 13 : Captions are not consistent with each other - Figures 14 and 19: make both captions consistent. Spectra of what? Measured where?

Done.

- Page 15, line 1: “determining the near wake” limit or boundary? - Page 15, line 3: “reveals”

Done.

- Figure 18 : Y axis is not consistent with the caption

Done.

- Conclusion: remind in the conclusion the used method to generate the turbulent inflow

Done.